NJC

PAPER

Complete and incomplete spin transitions in 1D chain iron(II) compounds†

Toni M. Pfaffeneder,[a] **Sebastian Thallmair,**[a] **Wolfgang Bauer**[a] **and Birgit Weber***[ab]

The synthesis and characterisation of two new octahedral iron(II) SCO coordination polymers [FeL1(bimm)] (**1**) and [FeL2(bppa)](MeOH)$_{0.5}$ (**2**) (L1 = [3,3']-[1,2-phenylenebis-(iminomethylidyne)]bis(4-phenyl-2,4-butanedionato)(2-)-$N,N',O^2,O^{2'}$], L2 = [*E,E*]-[{diethyl 2,2'-1,2-phenylenebis(iminomethylidyne)bis(3-oxo-3-phenylpropanato)}(2-)-N,N',O3,O3'], bimm = bis(1*H*-imidazol-1-yl)methane and bppa = 1,3-bis(pyridine-4-yl)propane) is presented. Results from X-ray structure analysis at different temperatures revealed in the case of **1** that the transition from a gradual to a cooperative SCO with a 5 K wide hysteresis is due to an increase of the short intermolecular contacts, which exceed a certain threshold for the cooperative effect. In the case of compound **2** an incomplete spin transition with a 4 K wide hysteresis was observed. The low temperature $\chi_M T$ product remains constant at a value typical for a mixed HS/LS state in stepwise spin transitions. A quantitative correlation between the cooperative effects of 12 monomer and polymer iron(II) SCO complexes and their structural properties derived from X-ray structure analysis, the so-called crystal contact index, CCI, is introduced.

Introduction

There is an ongoing interest in the bistability of spin crossover (SCO) compounds,[1] as the thermochromism associated with the spin transition (ST) makes them potentially useful for various applications such as display and memory device units,[2] sensors[3] and cold channel control units in food and medical storages.[4]

The origin of hysteresis loops in ST materials and their thermal width as well as the reason for stepwise or incomplete spin transitions are not yet fully understood. In the case of 1D chain SCO compounds, bridges with flexible linkers (triply bis-tetrazole bridges with flexible spacers[5] or flexible single bridges as 1,2-bis(4-pyridyl)ethane[6]) so far resulted in gradual ST. In the case of rigid linkers the ST behaviour depends on the intermolecular interactions (hydrogen bonds, π-stacking, van der Waals interactions) that are discussed to be suitable for transmitting cooperative interactions. This was recently demonstrated for 4,4'-bipyridine linked SCO complexes, where either gradual[7] or abrupt ST with 18 K wide thermal hysteresis loops[8] were obtained. A similar observation was made for triply 1,2,4-triazole bridged iron(II) complexes.[9]

Stepwise spin transitions are often associated with two or more non-equivalent iron centres. This was observed for the first 1D polymeric material undergoing a two-stepped spin transition recently presented by Neville, Murray and co-workers.[10] Of the two compounds presented, performing a step-wise spin transition, results from X-ray structure analysis revealed, that one ([Fe(NCS)$_2$(bdpp)], with bdpp = 4,6-bis(2',2''-pyridyl)pyrazine)), has two distinct iron(II) centres at each temperature with ordered, alternating HS and LS sites at the intermediate plateau (IP) temperatures. In contrast to this the second complex ([Fe(NCSe)$_2$(bdpp)]) has one unique iron(II) centre at each temperature with an averaged HS/LS character at the IP temperature. Great efforts were made by the authors to explain the 2-step spin transition in this compound.
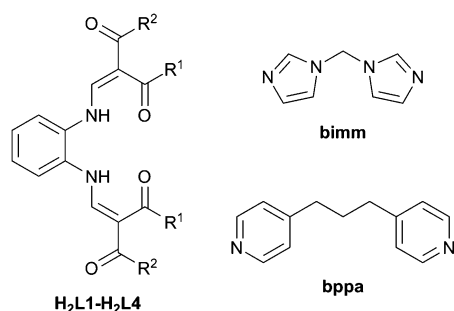
In this paper we present two examples for 1D chain iron(II) SCO complexes with flexible bridges, but a cooperative spin transition with small thermal hysteresis loops. The complexes are obtained by the combination of Schiff base-like equatorial tetradentate ligands H$_2$L1 and H$_2$L2 with the bridging axial ligands bimm (bis(1*H*-imidazol-1-yl)methane) and bppa (1,3-bis-(pyridine-4-yl)propane) (Scheme 1). The two equatorial ligands were so far not used for the synthesis of SCO complexes. They can be derived from the ligands H$_2$L3 and H$_2$L4, which were demonstrated to be highly suitable for the synthesis of SCO complexes,[11,12] by replacement of two of the methyl groups by phenyl groups. Bimm[13] and bppa[14] were already demonstrated to be suitable for the synthesis of SCO complexes of this ligand type.

In the last section of the manuscript a quantitative model is introduced to correlate the strength of the cooperative

---

a Center for Integrated Protein Science Munich at the Department Chemie und Biochemie, Ludwig-Maximilians-Universität München, B, u, tenandtstr. 5-13 (Haus F), D-81377 München, Germany

b Inorganic Chemistry II, Universität Bayreuth, Universitätsstraße 30, NW I, 95440 Bayreuth, Germany. E-mail: weber@uni-bayreuth.de; Fax: +49 92155-2157; Tel: +49 92155-2555

Scheme 1 Ligands used in this work. **H_2L1**: R^1 = Me, R^2 = Ph; **H_2L2**: R^1 = Ph, R^2 = OEt; **H_2L3**: R^1 = Me, R^2 = OEt; **H_2L4**: R^1 = Me, R^2 = Me.

interactions with the number and intensity of the intermolecular interactions.

Experimental

Materials

All syntheses were carried out under argon using Schlenk techniques. Methanol was purified as described in the literature and distilled under argon.[15] The synthesis of H_2L1,[16] H_2L2,[17] $[FeL2(MeOH)_2]$[18] and iron(II)acetate[19] is described in the literature.

The axial ligand bimm was prepared according to ref. 13, bppa was purchased from Aldrich Chemical Co. and used as-received.

Synthesis

$[FeL1(MeOH)_2]$. A mixture of anhydrous iron(II)acetate (2.04 g, 11.7 mmol) and H_2L1 (3.12 g, 6.90 mmol) in methanol (150 mL) was heated at reflux for 1 h. After cooling, the dark purple precipitate was filtered off, washed with methanol (2 × 5 mL) and dried in vacuum. Yield: 2.85 g (72%). Found: C, 63.1; H, 5.2; N, 4.9. Calc. for $C_{30}H_{30}FeN_2O_6$: C, 63.2; H, 5.3; N, 4.9%. IR (KBr/cm^{-1}): 1556s (CO). MS (DEI$^+$): m/z 507 (33, FeL1$^+$ + H$^+$), 506 (100, FeL1$^+$), 464 (6, FeL1$^+$ – COCH$_3$), 429 (4, FeL1$^+$ – C$_6$H$_5$), 105 (25, COC$_6$H$_5$$^+$), 77 (19, C$_6H_5$$^+$).

$[FeL1(bimm)]$ (1). A mixture of $[FeL1(MeOH)_2]$ (0.12 g, 0.21 mmol) and bimm (0.25 g, 1.66 mmol) in methanol (10 mL) was heated at reflux for 1 h. After cooling, the dark brown precipitate was filtered off, washed with methanol (1 × 3 mL) and dried in vacuum. Single crystals of **1** were slowly formed by diffusion techniques in methanol solution after several weeks. Yield: 0.09 g (65%). Found: C, 63.7; H, 4.6; N, 12.5. Calc. for $C_{35}H_{30}FeN_6O_4$: C, 64.2; H, 4.6; N, 12.8%. IR (KBr/cm^{-1}): 1557s (CO). MS (DEI$^+$): m/z 506 (45%, FeL1$^+$), 148 (66, bimm$^+$), 81 (100, bimm$^+$ – C$_3$H$_3$N$_2$), 43 (14, COCH$_3$$^+$).

$[FeL2(bppa)](MeOH)_{0.5}$ (2). A mixture of $[FeL2(MeOH)_2]$ $(MeOH)_{0.5}$ (0.29 g, 0.45 mmol) and bppa (0.25 g, 1.66 mmol) in methanol (20 mL) was heated at reflux for 1 h. After cooling, the black precipitate was filtered off, washed with methanol (2 × 5 mL) and dried in vacuum. Single crystals of **2** were slowly formed by diffusion techniques in methanol solution after several weeks. Yield: 0.23 g (65%). Found: C,

67.15; H, 5.2; N 7.3. Calc. for $C_{43.5}H_{42}FeN_4O_{6.5}$: C, 66.9; H, 5.4; N, 7.2%. IR (KBr/cm^{-1}): 1679vs (COO), 1552vs (CO). MS (DEI$^+$): m/z 567 (43%, FeL2 + H$^+$), 521 (13, FeL2$^+$ – OC$_2$H$_5$), 494 (13, FeL2$^+$ – OC$_2$H$_5$ – C$_2$H$_5$), 422 (6, FeL2$^+$ – 2 CO$_2$C$_2$H$_5$ + 2 H), 416 (5, FeL2$^+$ – OC$_2$H$_5$ – COC$_6$H$_5$), 371 (10, FeL2$^+$ – 2 OC$_2$H$_5$ – COC$_6$H$_5$), 198 (23, bppa$^+$), 106 (19, C$_7$H$_8$N$^+$), 105 (34, COC$_6$H$_5$$^+$), 93 (21, C$_6H_6$N + H$^+$), 92 (4, C$_6H_6N^+$), 78 (5, C$_5H_4N^+$), 77 (21, C$_6H_5$$^+$), 44 (7, OC$_2H_5$ – H$^+$), 29 (11, C$_2$H$_5$$^+$).

$[FeL2(bimm)](MeOH)_{0.5}$ (3). A mixture of $[FeL2(MeOH)_2]$ $(MeOH)_{0.5}$ (0.10 g, 0.16 mmol) and bimm (0.12 g, 0.79 mmol) in methanol (10 mL) was heated at reflux for 1 h. After cooling, the green precipitate was filtered off, washed with methanol (1 × 3 mL) and dried in vacuum. Yield: 0.08 g (68%). Found: C, 61.4; H, 4.7; N, 11.6. Calc. for $C_{37.5}H_{36}FeN_6O_{6.5}$: C, 61.65; H, 5.0; N, 11.5%. IR (KBr/cm^{-1}): 1668m, 1660m (COO), 1557s (CO). MS (FAB$^+$): m/z 714 (1%, M$^+$), 566 (4, M$^+$ – bimm).

Magnetic measurements

Magnetic susceptibility data were collected using a Quantum Design MPMSR-2 SQUID magnetometer under an applied field of 0.05 T over the temperature range 5–300 K. All samples were placed in gelatine capsules held within a plastic straw. The data were corrected for the magnetisation of the sample holder and the ligands using tabulated Pascal's constants.

X-Ray crystallography

The intensity data of **1** and **2** were collected on an Oxford XCalibur diffractometer using graphite-monochromated MoK_α radiation. The data were corrected for Lorentz and polarisation effects. The structure was solved by Direct Methods (Sir 97)[20] and refined by full-matrix least-square techniques against F_0^2 (SHELXL-97).[21] The hydrogen atoms were included at calculated positions with fixed displacement parameters. All non-hydrogen atoms were refined anisotropically. ORTEP-III was used for the structure representation.[22] Graphical representations of the molecular packing were done with SCHAKAL 99.[23] The crystallographic data are summarised in Table 6.†

Results and discussion

Synthesis

Scheme 1 displays the ligands used in this work. H_2L1 and H_2L2 were synthesised as previously described in the literature.[16,17] The 1D octahedral iron(II) coordination polymers could be obtained in a two-pot reaction. In a first step, iron complexes of the tetradentate equatorial ligands H_2L1 and H_2L2 with methanol as axial ligands were prepared starting from iron(II)acetate.[18] In a subsequent ligand substitution reaction $[FeL1(MeOH)_2]$ and $[FeL2(MeOH)_2]$ were converted with the axial-bridging ligands bimm and bppa, respectively, to give $[FeL1(bimm)]$ (**1**), $[FeL2(bppa)](MeOH)_{0.5}$ (**2**) and $[FeL2(bimm)](MeOH)_{0.5}$ (**3**) in good yields. The complexes were fully characterised by elemental analysis, IR and mass spectroscopy. X-Ray diffraction data could be obtained for **1** and **2**. The magnetic properties were determined by

T-dependent susceptibility measurements using a SQUID magnetometer.

Magnetic properties

Magnetic susceptibility measurements for all compounds were performed in the temperature range from 5–300 K. The thermal dependence of the product $\chi_M T$ (χ_M being the molar susceptibility and *T* the temperature) for **1** is displayed at the top of Fig. 1.

The room temperature value, $\chi_M T = 3.67$ cm^3 K mol^{-1}, is within the range expected for an iron(II) complex in the HS state. Upon cooling, the $\chi_M T$ product decreases first slowly until at 180 K about 30% of the iron centres are in the LS state. Below this point the remaining HS iron centres perform an abrupt transition into the LS state with $\chi_M T = 0.14$ cm^3 K mol^{-1} at 5 K. The critical temperatures are 171 K in the cooling and 176 K in the heating mode, corresponding to a 5 K wide thermal hysteresis loop.

The plot of $\chi_M T$ *versus* the temperature for complex **2** is given in the middle of Fig. 1. The room temperature value of $\chi_M T = 3.27$ cm^3 K mol^{-1} is typical for iron(II) in the HS state.
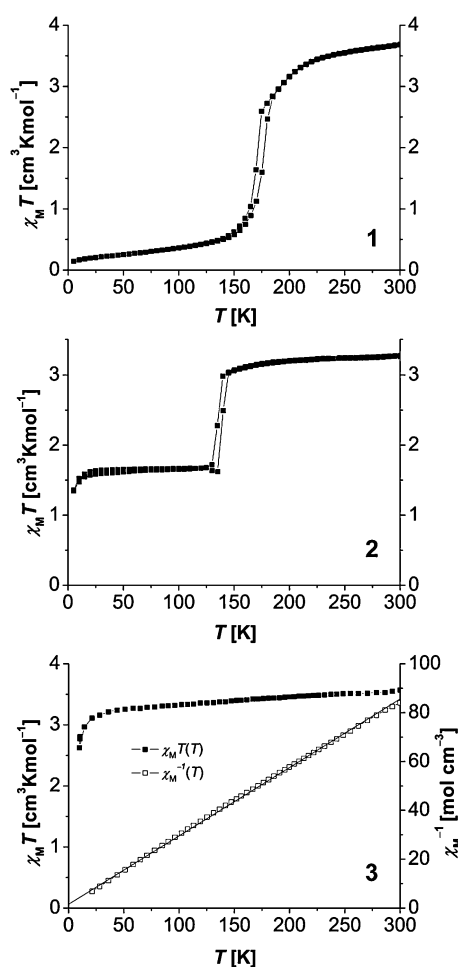

Fig. 1 Plots of the $\chi_M T$ product (filled squares) *vs.* *T* for compounds **1**, **2** and **3**. Reciprocal molar susceptibility χ_M^{-1} (open squares) as a function of *T* and the fit according to the Curie–Weiss law, $\chi_M = C/(T - \Theta)$, with the parameters $\Theta = -5.44$ K, $C = 3.57$ cm^3 K mol^{-1} for compound **3**.

Upon cooling the moment remains constant until about 180 K where a very abrupt ST takes place. A 4 K wide thermal hysteresis loop is observed with critical temperatures of 136 K upon cooling and 140 K upon heating. In the low temperature region a mixed HS/LS state is obtained with $\chi_M T = 1.58$ cm^3 K mol^{-1}. For compound **3** (bottom of Fig. 1) nearly ideal Curie behaviour is observed. Upon cooling the $\chi_M T$ product decreases from a value of 3.56 cm^3 K mol^{-1} at 295 K to a value of 3.08 cm^3 K mol^{-1} at 20 K. The susceptibility data above 20 K can be fitted very well with the Curie–Weiss law ($\chi_M = C/(T - \Theta)$) with the parameters $\Theta = -5.44$ K and $C = 3.57$ cm^3 K mol^{-1}. The Curie constant *C* is in a region expected for iron(II) HS complexes and the negative Weiss constant Θ in combination with the temperature dependent decrease of the $\chi_M T$ product could be an indication for weak antiferromagnetic interactions between the chains, but other reasons are also possible. This is a typical behaviour for an HS iron(II) complex of this ligand type.[24]
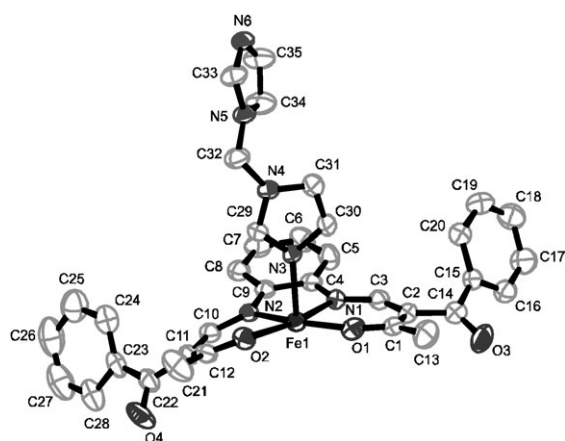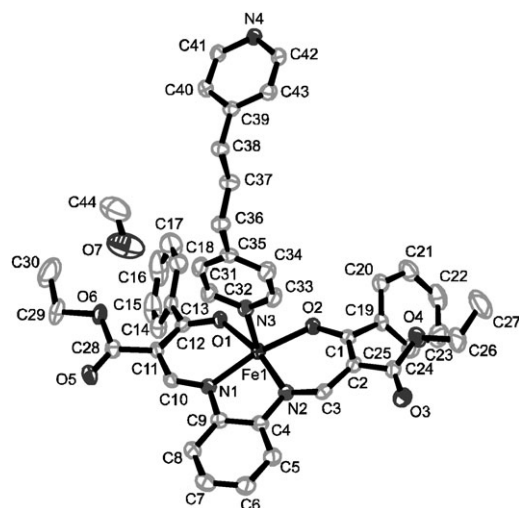
Structural descriptions

Crystals suitable for X-ray structure analysis were obtained for both spin crossover complexes **1** and **2**. The crystallographic data are summarised in Table 6. Selected bond lengths and angles within the first coordination sphere are summarised in Table 1. ORTEP representations of the HS forms of **1** and **2** are given in Fig. 2 and 3, respectively. In the case of **1**, the X-ray structure was measured at three temperatures before (250 K), during (180 K) and after the spin transition (125 K). In the case of **2** a determination of the X-ray structure was only possible for the HS state as the crystals crumble while cooling down.

Intramolecular changes upon spin transition of 1. In the HS state the average bond lengths within the first coordination sphere of **1** are 2.09 Å (Fe–N$_{eq}$), 2.03 Å (Fe–O$_{eq}$) and 2.22 Å (Fe–N$_{ax}$). The values are within the region reported for HS iron(II) complexes of the same ligand type.[11–14] Upon spin transition a shortening of the bond lengths of about 10% is observed, as discussed for other iron(II) spin crossover complexes in the literature.[1] This shortening is more pronounced for the axial ligands, which connect the iron centres in the 1D chain, than for the equatorial ones in agreement with previous findings on mononuclear analogues.[11–14] The average bond lengths in the LS state are 1.91 Å (Fe–N$_{eq}$), 1.93 Å (Fe–O$_{eq}$) and 2.02 Å (Fe–N$_{ax}$). A characteristic tool for the determination of the spin state of this type of iron(II) complexes is the O–Fe–O angle that changes from 109° in the HS state to 91° in the LS state.[11,14] The 1D chain of compound **1** is linear, with the equatorial ligands being parallel to each other within one chain (Fig. 4, at the top).

Intermolecular interactions of 1. Selected intermolecular distances for the 250 K, 180 K and 125 K structure of **1** are shown in Table 2. Selected views of the molecule packing of **1** in the crystal at 250 K and 125 K are given in Fig. 5. Between 200 K and 180 K compound **1** undergoes a gradual spin transition with no indications for cooperative interactions. Then upon further cooling an abrupt transition with a 5 K wide hysteresis occurs. The initial gradual transition is

Table 1 Selected bond lengths [Å] and angles [°] within the first coordination sphere of **1** at 125 K, 180 K and 250 K and of **2** at 173 K

Complex	T/K	S	Fe–N$_{eq}$	Fe–O$_{eq}$	Fe–L$_{ax}$	O1–Fe–O2	L$_{ax}$–Fe–L$_{ax}$
1	250	2	2.090(3), 2.099(3)	2.028(3), 2.027(2)	2.205(3), 2.225(3)	109.47(10)	171.44(11)
1	180	2/0	2.049(3), 2.070(3)	2.014(3), 2.005(3)	2.159(3), 2.177(3)	106.69(11)	172.00(12)
1	125	0	1.910(4), 1.919(4)	1.931(3), 1.936(3)	2.017(3), 2.017(3)	91.43(13)	175.21(13)
2	173	2	2.093(1), 2.083(1)	2.004(1), 2.013 (1)	2.231(1), 2.249(1)	106.56(5)	177.26(5)

Fig. 2 ORTEP drawing of the asymmetric unit of **1** at 250 K. Hydrogen atoms were omitted for clarity. Thermal ellipsoids are shown at the 50% probability level.

Fig. 3 ORTEP drawing of the asymmetric unit of **2** at 173 K. Hydrogen atoms were omitted for clarity. Thermal ellipsoids are shown at the 50% probability level.

Fig. 4 Top: excerpt of the 1D polymeric chain of compound **1** in the crystal at 250 K, view along [001]; bottom: a zigzag motif of the 1D polymeric chain of compound **2** in the crystal at 173 K, view along [100]. Hydrogen atoms have been omitted for clarity.

Table 2 Selected intermolecular distances (*d*) [Å] and differences between atomic distances and the sum of the van der Waals radii (vdW) [Å] of **1** at 250 K, 180 K and 125 K

	T/K	d	d − vdW
C29–H29···O3[a]	250	2.26	−0.46
	180	2.24	−0.48
	125	2.42	−0.30
C32–H32B···O2[b]	250	2.48	−0.24
	180	2.43	−0.29
	125	2.51	−0.21
C7···C8[c]	180	3.28	−0.12
C7···C8[c]	125	3.19	−0.21
C31–H31···O4[d]	125	2.46	−0.26
C32–H32B···O1[b]	125	2.49	−0.23
C13–H13A···O4[e]	125	2.57	−0.15
H13A···H21B[e]	125	2.27	−0.13
C32–H32A···C15[f]	125	2.78	−0.12
C34···C18[a]	125	3.29	−0.11
C17–H17···C8[a]	125	2.79	−0.11
H21A···H21B[g]	125	2.30	−0.10

[a] −1 + x, y, z. [b] 1 − x, −y, 1 − z. [c] 1 − x, 1 − y, − z. [d] −1 + x, 1 + y, z. [e] 1 − x, 1 − y, 1 − z. [f] 1 + x, y, z. [g] −x, 1 − y, 1 − z.

explained by the presence of only a few short intermolecular contacts in the high temperature structure (see Fig. 5, 250 K). Upon cooling the number of short contacts increases. The 180 K structure has one additional contact besides the other more shortened contacts in comparison to the 250 K structure. This increases the total communication of elastic interactions and accounts for a certain threshold value for the occurrence of the observed cooperative effect. The additional contact (C7···C8) in the 180 K structure facilitates the π-stacking of the 1,2-disubstituted benzene ring of the equatorial ligand between adjacent chains and makes the interaction network

three-dimensional. The low temperature structure (125 K) is characterised by many additional short intermolecular contacts which satisfactorily explain the small hysteresis observed in the magnetic measurements.

Discontinuous spin transitions were recently associated with order/disorder transitions of counter ions[25] or additional ligand molecules[26] in the crystal packing. The order/disorder transition at a certain temperature facilitated a significant increase in the number of intermolecular contacts below this
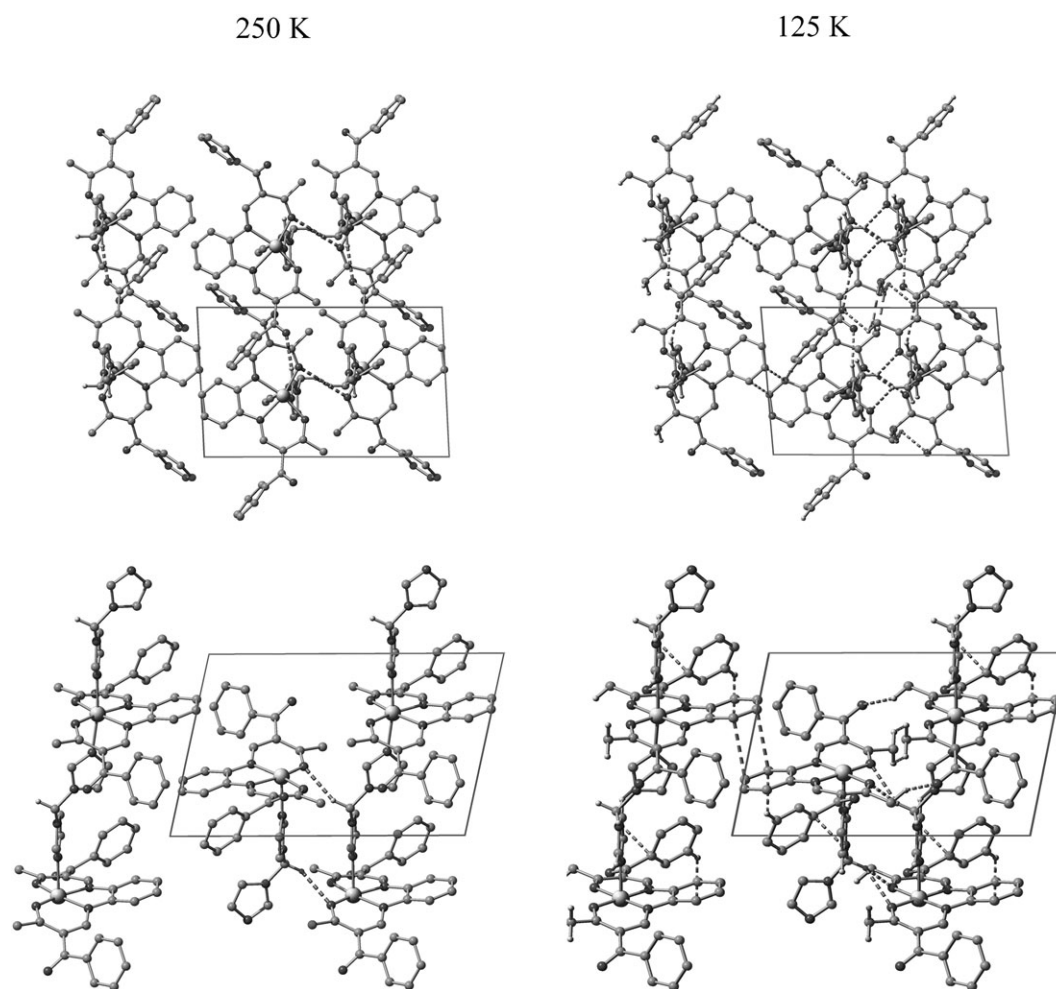
250 K   125 K

Fig. 5 Left: packing of compound **1** in the crystal at 250 K; right: packing at 125 K; top: view along [010], bottom: view along [100]. Hydrogen atoms, which do not participate in short intermolecular interactions, have been omitted for clarity. Crystal contacts shorter than the sum of the van der Waals radii minus 0.1 Å are depicted with dashed bonds.

temperature that exceeds a threshold and therefore mediates the cooperative effect. Compound **1** does not exhibit an additional disordered counter ion, solvent or ligand molecule or any other disordered parts. Thus only the number and the nature (or strength) of the intermolecular interactions are important for the discussion of cooperative interactions.

A zigzag motif in the crystal structure of 2. The average bond lengths within the first coordination sphere of **2** are 2.09 Å ($Fe-N_{eq}$), 2.01 Å ($Fe-O_{eq}$) and 2.24 Å ($Fe-N_{ax}$). The values are within the region reported for HS iron(II) complexes as discussed above (see Table 1).[11–14] The O–Fe–O angle is with 107° clearly in the range typical for a HS complex. Selected intermolecular distances of **2** are summarised in Table 3. In Fig. 4 the 1D polymeric chain of octahedral iron(II) centres (at the bottom) and in Fig. 6 the packing of the chains in the crystal are displayed. The 1D chain of **2** exhibits a zigzag motif with an angle between two adjacent equatorial ligands of 99°. Such motifs were previously found in the crystal structure of the closely related [FeL3(bppa)] and [FeL4(bppa)](MeOH) (see Scheme 2).[14,27] The first compound undergoes an incomplete spin transition that stops at an intermediate plateau (IP) while
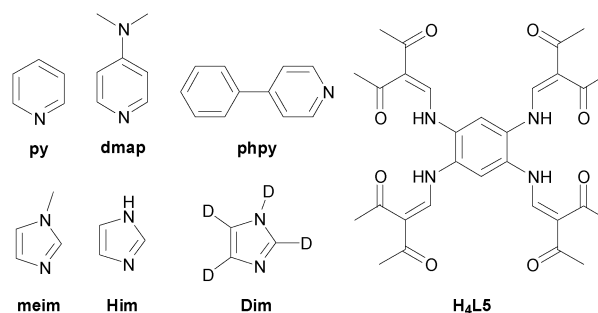
the latter compound undergoes a stepwise thermal spin transition with a very wide step. It could be deduced from the structures and the structures of related 1D chain SCO complexes that the zigzag motif of the 1D chain as well as a dense packing (intermolecular contacts shorter than the sum of the van der Waals radii) are responsible for restraining interactions between these chains and hence stabilise the mixed HS/LS state of the step.[14,30] In general, a HS → LS transition in 1D chain compounds involves a relocation of the ligands towards the smaller LS molecule. If the Fe···Fe distances cannot follow the changes in Fe–L bonds due to restraining interactions, a stabilisation of a mixed HS/LS state can be observed.[14,28] For zigzag chains restraining intermolecular interactions can be more easily imagined compared to linear structures and therefore wider steps can be expected.[14] The spin transition behaviour of **1** and **2** is in agreement with this idea. In the case of the linear chain compound **1** a one-stepped ST is observed while for **2** the ST stops at the IP (see Fig. 1 and 4). Compound **2** differs only in one homotopic residue from the previously published [FeL3(bppa)] and in two homotopic residues from the previously published [FeL4(bppa)](MeOH). Instead of two methyl-groups in L3 and L4 it contains two

Table 3 Selected intermolecular distances (*d*) [Å] and differences between atomic distances and the sum of the van der Waals radii (vdW) [Å] of **2** at 173 K

	d	*d* − vdW
O7–H7···O6	2.12	−0.60
C24–H24···O5[a]	2.50	−0.22
C44–H44B···O4[b]	2.53	−0.19
C41–H41···O3[b]	2.56	−0.16
C38–H38B···O1[c]	2.59	−0.13
C16–H16···O7[d]	2.59	−0.13
C7···C9[e]	3.43	+ 0.03

[a] 1/2 + *x*, 1/2 − *y*, 1 − *z*. [b] −1/2 + *x*, *y*, 1/2 − *z*. [c] 1 − *x*, 1/2 + *y*, 1/2 − *z*. [d] 3/2 − *x*, 1/2 + *y*, *z*. [e] 1 − *x*, −*y*, 1 − *z*.

Scheme 2 Further ligands discussed in this work.

sterically more demanding phenyl-groups in the equatorial ligand, which are distorted out of the plane. The second difference between L2 and L4 is two ethoxycarbonyl-groups instead of two methylcarbonyl-groups. In contrast to [FeL3(bppa)] (abrupt incomplete one-stepped spin transition)[31] and [FeL4(bppa)](MeOH) (gradual two-stepped spin transition),[14] compound **2** shows a very abrupt but incomplete spin transition with a small hysteresis. The distorted phenyl-groups may increase the extent of restraining interactions within the zigzag structure and by this prevent the ST of the second half of the iron centres. Furthermore, the two ethoxycarbonyl-groups of the equatorial ligand provide an intertwining of adjacent chains (see Fig. 6, left), which are closely connected by several short contacts. Moreover, π-stacking of the 1,2-disubstituted benzene-rings of the equatorial ligand of two adjacent chains (Fig. 6, right) may become the most restraining interaction for the ligand relocation along [001] due to the usually pronounced shortening of the axial bond lengths. Very likely, all these interactions explain the remaining in the mixed HS/LS state through the whole low temperature range as well as the small hysteresis loop.

Crystal contacts mediate cooperative effects beyond a threshold

There are several examples that demonstrate that the number and intensity of contacts shorter than the sum of the van der Waals radii correlate with the cooperative nature of the spin transition.[14,29] The idea of a threshold for elastic interactions mediating cooperative effects in a spin crossover compound led us to the question, if there is a quantitative way to describe structural features. We discovered a simple approach to correlate the sum of short contacts of selected structures with the strength of the cooperative effect (gradual, abrupt or accompanied by hysteresis). Thereby we assume that every short contact (shorter than the sum of the van der Waals radii) contributes to the elastic interactions mediating the cooperative effect. Those which are very short (non-classical and classical H-bonds) contribute more to the cooperative effect than those which are longer (π-stacking, van der Waals contacts). Eqn (1) combines all these assumptions. The crystal contact index (CCI) is the sum of all short and weighted contacts. The differences between the sum of the van der Waals radii (vdW) and the atomic distances of the contacts (*d*) were obtained using the program MERCURY 2.2[30] and were weighted by an exponential function, in which very short

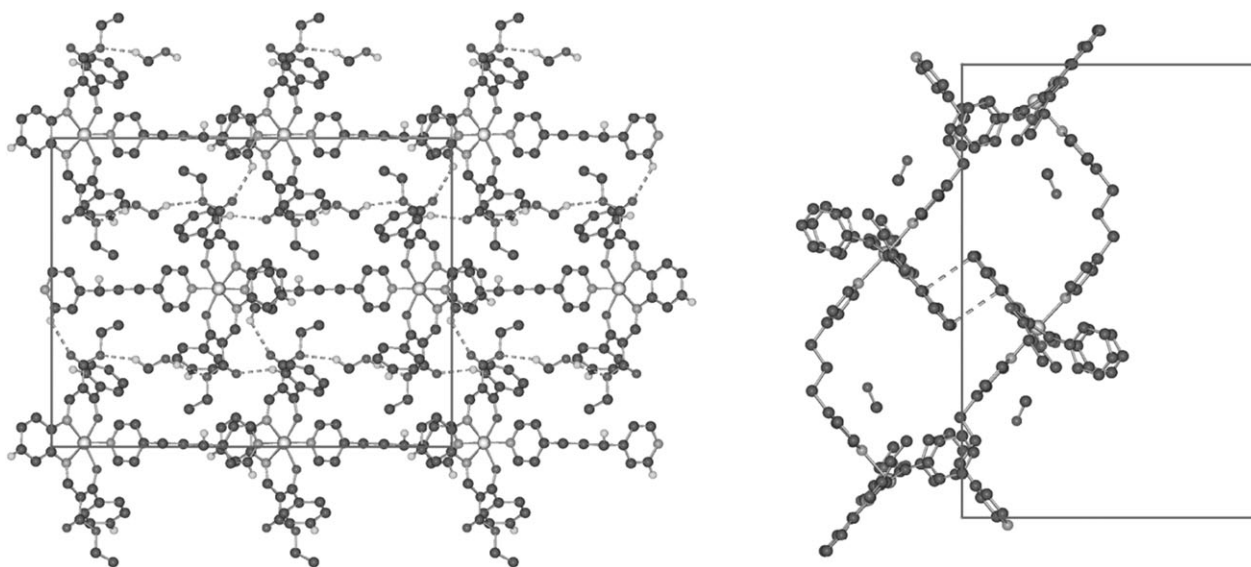**Fig. 6** Left: excerpt of a 2D layer of parallel chains of **2** in the crystal packing, view along [010]; right: π-stacking of the equatorial ligands of two adjacent chains of **2**, view along [100]. Hydrogen atoms, which do not participate in short intermolecular interactions, have been omitted for clarity. Crystal contacts shorter than the sum of the van der Waals radii minus 0.1 Å are depicted with dashed bonds.

Table 4 Correlation between cooperative effects and structural analysis of selected spin crossover compounds of the Jäger-ligand system. Type: m = monomeric, d = dimeric, p = 1D polymeric coordination compound; HS = high-spin structure, LS = low spin-structure; CCI = crystal contact index; Δa, Δb, Δc = percentage difference in cell parameter change upon spin transition; AP = anisotropy parameter; CI = crystal index

No.	Compound	Ref.	Type	S	Feature	Hys. Width/K	CCI	Δa (%)	Δb (%)	Δc (%)	AP	CI
1	[FeL1(bimm)]	This work	p	HS [HS] > [LS] LS	Gradual, then hys.	5	1.2 1.5 2.2	0.6	−3.8	−2.3	3.3	7.3
2	[FeL2(bppa)] (MeOH)$_{0.5}$	This work	p	HS	Hys., incompl.	4	2.0					
4	[FeL3(py)$_2$]	32	m	HS LS	Gradual		0.7 1.0	−1.1	−0.9	−1.5	0.1	0.1
5	[FeL3(phpy)$_2$]	12d	m	HS LS	Gradual, then hys.	4	1.2 2.0	0.6	0.6	−2.6	2.3	4.6
6	[FeL4(py)$_2$]	12a	m	HS LS	Hys.	2	0.9 1.0	0.0	−1.0	−3.8	2.6	2.6
7	[FeL4(phpy)$_2$] (phpy)	12d	m	LS	Gradual		1.5					
8	[FeL4(meim)$_2$] (meim)	26	m	HS LS	Hys., then gradual	2	1.8 1.4	−0.9	−1.2	−1.1	0.0	0.0
9	[FeL4(dmap)$_2$]	12a	m	HS	Hys	9	0.6					
10	[Fe$_2$(L5)(meim)$_4$] (meim)$_2$	26	d	LS	Gradual, then hys.	21	2.5	−3.1	−3.8	−2.4	0.3	0.75
11	[FeL3(Him)$_2$]	33	m	HS	Hys.	70	4.1					
12	[FeL3(Dim)$_2$]	34	m	HS	Hys.	66	4.0					
13	[FeL3(Him)$_2$], second modification	35	m	LS	Hys.	4	4.2					

contacts are more pronounced. Table 4 gives an overview of the selected compounds, which were analysed by this method. The further ligands which are mentioned therein and in the following are displayed in Scheme 2.

For compound **1** the CCI values represent the results made in the preceding section by analysis of the crystal packing. Upon cooling, the CCI value increases from 1.2 (250 K) to 1.5 (180 K) and finally to 2.2 (125 K) indicating that the strength and the number of short contacts increase. Below 180 K the threshold value for the elastic interactions seems to be reached and the remaining HS centres perform now a cooperative spin transition. The CCI thus helps to explain the observed spin transition. A similar behaviour as for **1** was observed for compound **5** ([FeL3(phpy)$_2$], HS: 1.2, LS: 2.0)[12d] with a similar curve progression while an opposite trend was observed for the previously published compound **8** ([FeL4(meim)$_2$] (meim)).[26] Here the CCI value for the HS structure (1.8) is higher than the value for the LS structure (1.4). Although the number of short contacts increases upon cooling, the intensity of the contacts decreases. This is in good agreement with the results from the magnetic measurements where a 2 K wide thermal hysteresis loop is observed in the beginning and a more gradual character is observed in the second part of the transition curve.[26]

$$CCI = \sum_{x>0} (e^{x_n^{3/2}} - 1)$$ (1)

$$x = \frac{vdW - d}{[\text{Å}]} > 0$$

$$AP = Var(\Delta a, \Delta b, \Delta c) \times 10^4 = \frac{\sum (x - \bar{x})^2}{n} \times 10^4$$ (2)

$$\Delta a = 1 - \frac{a_{HS}}{a_{LS}}; \Delta b = 1 - \frac{b_{HS}}{b_{LS}}; \Delta c = 1 - \frac{c_{HS}}{c_{LS}}$$

$$CI = AP \cdot CCI$$ (3)

On the basis of the data in Table 4, it can be concluded that low cooperativity can be expected for CCI-values between
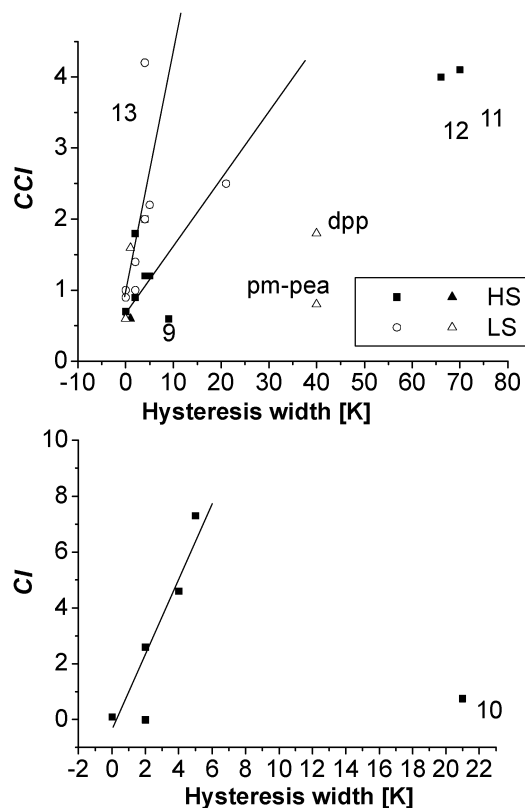

Fig. 7 Plots of the crystal contact index (CCI) (top) and the crystal index (CI, at the bottom) against the hysteresis width. Values are taken from Table 4 (circles and squares) and from the text (triangles, literature examples).

0 and 1.5, medium cooperativity between 1.0 and 2.0 and high cooperativity for values higher than 2.0. This general trend is visualised on top of Fig. 7.

The CCI value is not only useful to explain the curve progression of spin transition curves, it can also be used to estimate if solvent molecules included in the crystal packing

Table 5 Selected CCI values corrected by disregarding of the short contacts provided by additional solvent or ligand molecules in the crystal structure (compare with Table 4)

	Add. molecule	S		CCI (eqn (1))	CCI (corr.)	Comment on correction
7	Phpy	LS	Grad.	1.5	0.9	Better value; dilution effect
8	Meim	HS	2 K hys.	1.8	1.0	Value too low; meim contributes to the cooperative effect
		LS		1.4	0.8	
2	0.5 MeOH	HS	4 K hys.	2.0	0.5	Value too low; MeOH contributes to the cooperative effect

Table 6 Crystallographic data of **1** and **2** discussed in this work

Complex	**1** (125 K)	**1** (180 K)	**1** (250 K)	**2**
Empirical formula	$C_{35}H_{30}FeN_6O_4$			$C_{43.54}H_{42.17}FeN_4O_{6.54}$
Formula weight	654.50			782.01
T/K	125(2)	180(2)	250(2)	173(2)
Crystal size/mm	$0.27 \times 0.11 \times 0.05$	$0.26 \times 0.11 \times 0.05$	$0.26 \times 0.11 \times 0.05$	$0.41 \times 0.34 \times 0.22$
Crystal system	Triclinic	Triclinic	Triclinic	Orthorhombic
Space group	$P\bar{1}$	$P\bar{1}$	$P\bar{1}$	$Pbca$
λ/Å	0.71073	0.71073	0.71073	0.71073
a/Å	10.4117(14)	10.3326(16)	10.3530(16)	19.3122(4)
b/Å	10.5247(12)	10.8298(17)	10.928(2)	16.5116(3)
c/Å	15.4338(18)	15.672(3)	15.794(4)	25.1186(5)
α/°	74.913(10)	74.763(14)	75.074(19)	90
β/°	79.006(11)	80.991(14)	81.233(17)	90
γ/°	64.091(13)	64.329(15)	64.423(18)	90
V/Å^3	1463.0(3)	1523.2(4)	1555.7(5)	8009.7(3)
Z	2	2	2	8
ρ_{calc}/g cm^{-3}	1.486	1.427	1.397	1.297
μ/mm^{-1}	0.569	0.546	0.535	0.430
F(000)	680	680	680	3278
Θ range/°	3.83–25.35	3.74–25.35	3.76–25.35	4.20–26.28
Index ranges	$-13 \leq h \leq 13$	$-12 \leq h \leq 12$	$-13 \leq h \leq 12$	$-24 \leq h \leq 24$
	$12 \leq k \leq 13$	$-13 \leq k \leq 13$	$-14 \leq k \leq 14$	$-20 \leq k \leq 10$
	$19 \leq l \leq 19$	$-18 \leq l \leq 18$	$-19 \leq l \leq 20$	$-18 \leq l \leq 31$
Reflections collected	17 191	17 037	17 523	33 558
Reflections unique	5339 (R_{int} = 0.0819)	5537 (R_{int} = 0.0631)	5624 (R_{int} = 0.0634)	8121 (R_{int} = 0.0379)
R_1 (all)	0.0635 (0.1183)	0.0567 (0.1025)	0.0484 (0.0946)	0.0325 (0.0664)
wR_2	0.1494	0.1243	0.1179	0.0744
GooF	1.025	1.002	0.960	0.841

contribute to the cooperative effects or have a dilution effect. Such dilution effects are well known in spin crossover research and have been for example demonstrated for a series of mixed crystals with the general composition $[M_{1-x}Fe_x(pic)_3]X_2 \cdot solv$ (solv = MeOH, EtOH; X = Cl, Br; M = Co, Zn, Mn) with decreasing X.[31] The relative high LS-CCI-value for compound **7** ($[FeL4(phpy)_2]$ (phpy), 1.5)[12d] with an additional non-coordinated ligand molecule phpy can clearly be explained with a dilution effect of the additional phenylpyridine, as given in Table 5. In the case of compound **8**[26] or compound **2** the CCI values corrected by the solvent distribution (Table 5) are too low—here the molecules clearly contribute to the cooperative effects. For compound **2** the additional methanol molecules cross-link three different zigzag chains in the structure and contribute with three short contacts, containing a strong H-bond (O7–H7···O6), to the cooperative effect without a doubt (see Table 3).

Of course these values can only be seen as rough guidelines with exceptions due to many factors which cannot easily be quantified. Examples for such exceptions are compounds **9**[12a] and **11–13**,[34–36] see Fig. 7, top. In the case of **9** the CCI value leads to a clear underestimation of the hysteresis width, whereas for the compounds **11–13** the CCI value is in the same order of magnitude but very different hysteresis widths are obtained.[35] In the case of **13** an agreement with the steeper branch of the correlation could be discussed, for **11** and **12** again the hysteresis width is underestimated. Obviously additional factors contribute to the cooperative interactions in the case of **9**, **11** and **12**. Interestingly, for all four complexes hydrogen bonds are observed that involve an oxygen atom directly coordinated to the metal centre, as illustrated in Fig. 8 for **9** and **11**. Further ongoing investigations are in progress to more clearly analyse the influence of hydrogen bonds on cooperative interactions in spin crossover systems.

Guionneau *et al.* reported that very large and anisotropic unit cell modifications and the SCO phenomenon are probably indissociable. The unit cell temperature dependence evidences the amplitude of the strong structural rearrangement that accompanies the SCO as well as the hysteresis width.[36] Therefore we applied eqn (2) on the percentage change in the cell parameters a, b and c of compounds whose HS and LS structures are known (Table 4). Eqn (2) simply calculates the variance of the cell parameter change giving the value of the anisotropy parameter (AP). As the variance is a measure of the amount of variation within the values of a variable it could be seen as a measure of the anisotropy of the parameter
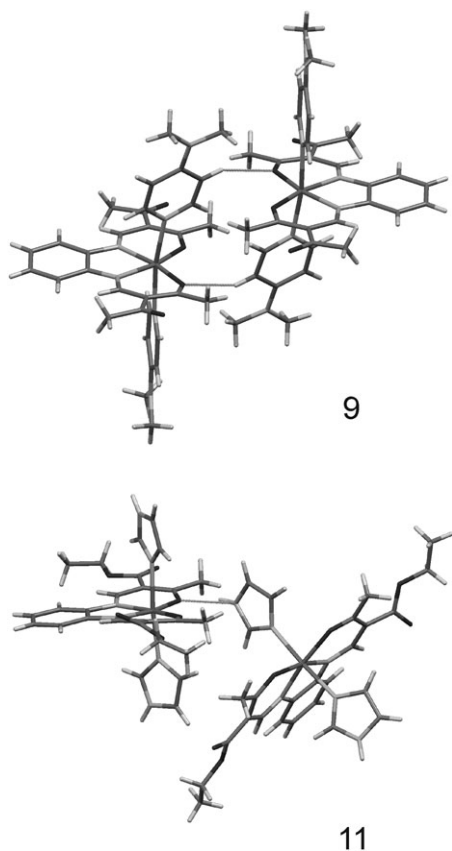
Fig. 8 Excerpt of the crystal packing of **9** (top) and **11** (bottom).

change in this particular case. This approach provides also a good correlation between the observed cooperative effect and the AP value. If the value is very low, the anisotropy in the cell parameter change is low as well as the cooperative effect (*e.g.* the value is 0.1 for the gradual SCO complex **4** in comparison to 3.3 for compound **1**).

Since there are some deviations, eqn (1) and (2) are combined by eqn (3) to give the crystal index (CI), which is the product of both parameters CCI and AP. Eqn (3) provides an improved correlation as can be seen in Table 4 and at the bottom of Fig. 7. A nearly linear dependency is observed for the compounds with smaller hysteresis loops, while complex **10** ([Fe$_2$(L5)(meim)$_4$] (meim)$_2$, 21 K wide hysteresis loop)[26] no longer fits into the correlation, probably because of its dinuclear nature. At this point it should be noted that no difference is observed between the mononuclear complexes and the polymer chain compounds with flexible linkers. A disadvantage in using AP and CI values is the limited availability of high- and low-spin structures of a particular complex due to crystal damages during the spin transition. In contrast, the CCI scale could be used for each structure. The concept of the CCI was tested on four SCO complexes that belong to the series [FeL$_2$(NCS)$_2$] with L = btz[37] (2,2′-bis-4,5-dihydrothiazin, gradual spin transition), phen[38] (1,10-phenanthrolin, abrupt spin transition), dpp (dipyrido[3,2-*a*:2′3′-*c*]phenazine, hysteresis 40 K) and pm-pea[36] (*N*-2′-pyridylmethylene-4-phenylethynyl, hysteresis 40 K). For this series the increasing cooperative interactions are correlated with an increasing number of intermolecular contacts.[29] Indeed, the CCI of

the first three complexes rises from 0.6 (btz) over 1.6 (phen) to 1.8 (dpp). The values of the first two compounds (btz and phen) fit nicely into the correlation given at the top of Fig. 7, while the value for the system [Fe(dpp)$_2$(NCS)$_2$] is too low, indicating that π-stacking probably cannot be expressed solemnly by the number of intermolecular contacts. This suggestion is reinforced by the last example (pm-pea) where a significantly lower CCI of 0.8 is obtained although the hysteresis width is similar to those of the dpp complex.

Conclusions

In this work we have presented the synthesis and characterisation of two new octahedral iron(II) SCO coordination polymers. Results from X-ray structure analysis at different temperatures revealed in the case of **1** that the transition from a gradual to a cooperative SCO with a 5 K wide hysteresis is due to an increase of the short intermolecular contacts, which exceed a certain threshold for the cooperative effect. In the case of compound **2** an incomplete spin transition with a 4 K wide hysteresis was observed. The low temperature $\chi_M T$ product remains constant at a value typical for a mixed HS/LS state in stepwise spin transitions. The structure of the 1D polymeric chain of **2** exhibits a further zigzag motif, which was previously found in related compounds with a stepwise or incomplete spin transition.[14,31] Restraining interactions provided by the zigzag motif as well as additional restraining interactions of the equatorial ligand may stabilise the mixed HS/LS state and make a further progression of the spin transition impossible.

Furthermore we established a correlation between the cooperative effects of 12 iron(II) SCO complexes and their structural properties derived from X-ray structure analysis, the so-called crystal contact index, CCI. For small hysteresis loops this correlation is in agreement with the model of elastic interactions mediating the structural rearrangements during the cooperative spin transition in the solid phase. It provides a good estimation to accompany the structural interpretation of spin transition properties and can to some extend also be applied to other SCO systems. In the case of spin transition compounds with wider hysteresis loops the correlation fails, indicating that there are additional mechanisms responsible for cooperative interactions. The clarification of the exact nature of those factors will be the topic of subsequent work.

Notes and references

1 (*a*) H. A. Goodwin, *Coord. Chem. Rev.*, 1976, **18**, 293; (*b*) E. König, *Struct. Bonding (Berlin, Ger.)*, 1991, **76**, 51; (*c*) P. Gütlich, A. Hauser and H. Spiering, *Angew. Chem., Int. Ed. Engl.*, 1994, **33**, 2024, and references therein; (*d*) *Spin Crossover in Transition Metal Compounds I–III*, in *Topics in Current Chemistry*, ed. P. Gütlich and H. A. Goodwin, Springer-Verlag, Berlin, Heidelberg, New York, 2004; (*e*) J. A. Real, A. B. Gaspar and M. C. Munoz, *Dalton Trans.*, 2005, 2062; (*f*) K. Nakano, N. Suemura, K. Yoneda, S. Kawata and S. Kaizaki, *Dalton Trans.*, 2005, 740; (*g*) O. Sato, J. Tao and Y.-Z. Zhang, *Angew. Chem.*, 2007, **119**, 2200 (*Angew. Chem., Int. Ed.*, 2007, **46**, 2152); (*h*) J. A. Kitchen and S. Brooker, *Coord. Chem. Rev.*, 2008, **252**, 2072; (*i*) K. S. Murray, *Eur. J. Inorg. Chem.*, 2008, 3101; (*j*) M. A. Halcrow, *Coord. Chem. Rev.*, 2009, 2059; (*k*) S. Brooker and J. A. Kitchen, *Dalton Trans.*, 2009, **253**, 2493; (*l*) C. J. Kepert, *Aust. J. Chem.*, 2009, **62**, 1079; (*m*) K. S. Murray, *Aust. J. Chem.*, 2009, **62**, 1081; (*n*) A. B. Koudriavtsev and W. Linert, *J. Struct. Chem.*, 2010, **51**, 335.

2 (*a*) O. Kahn and C. Jay Martinez, *Science*, 1998, **279**, 44; (*b*) O. Kahn, C. Jay, J. Kröber, R. Claude and F. Grolière, *Patent EP* 0666561, 1995; (*c*) J.-F. Létard, O. Nguyen, N. Daro, *Patent FR* 0512476, 2005; (*d*) J.-F. Létard, P. Guionneau and L. Goux-Capes, *Topics in Current Chemistry*, ed. P. Gütlich et and H. A. Goodwin, Springer, Wien, New York, 2004, vol. 235, p. 221; (*e*) A. Galet, A. B. Gaspar, M. C. Munoz, G. V. Bukin, G. Levchenko and J. A. Real, *Adv. Mater.*, 2005, **17**, 2949.

3 Y. Garcia, V. Kseofontov and P. Gütlich, *Hyperfine Interact.*, 2002, **139/140**, 543.

4 Y. Garcia, V. Kseofontov, S. Mentior, M. M. Dirtu, C. Gieck, A. Bhatthacharjee and P. Gütlich, *Chem.–Eur. J.*, 2008, **14**, 3745.

5 P. J. van Koningsbruggen, Y. Garcia, O. Kahn, L. Fournès, H. Kooijman, A. L. Spek, J. G. Haasnoot, J. Moscovici, K. Provost, A. Michalowicz, F. Renz and P. Gütlich, *Inorg. Chem.*, 2000, **39**, 1891.

6 G. S. Matouzenko, M. Perrin, B. le Guennic, C. Genre, G. Molnar, A. Bousseksou and S. A. Borshch, *Dalton Trans.*, 2007, 934.

7 (*a*) G. S. Matouzenko, G. Molnar, N. Brefuel, M. Perrin, A. Bousseksou and S. A. Borshch, *Chem. Mater.*, 2003, **15**, 550; (*b*) C. Genre, G. S. Matouzenko, E. Jeanneau and D. Luneau, *New J. Chem.*, 2006, **30**, 1669.

8 (*a*) B. Weber, R. Tandon and D. Himsl, *Z. Anorg. Allg. Chem.*, 2007, **633**, 1159; (*b*) B. Weber, E. S. Kaps, C. Desplanches and J.-F. Létard, *Eur. J. Inorg. Chem.*, 2008, 2963.

9 M. M. Dirtu, C. Neuhausen, A. D. Naik, A. Rotaru, L. Spinu and Y. Garcia, *Inorg. Chem.*, 2010, **49**, 5723.

10 (*a*) S. M. Neville, B. A. Leita, G. J. Halder, C. Kepert, B. Moubaraki, J.-F. Letard and K. S. Murray, *Chem.–Eur. J.*, 2008, **14**, 10123.

11 B. Weber and E.-G. Jäger, *Eur. J. Inorg. Chem.*, 2009, 465.

12 (*a*) B. Weber, E. Kaps, J. Weigand, C. Carbonera, J.-F. Letard, K. Achterhold and F.-G. Parak, *Inorg. Chem.*, 2008, **47**, 487; (*b*) B. Weber, E. S. Kaps, J. Obel and W. Bauer, *Z. Anorg. Allg. Chem.*, 2008, **634**, 1421; (*c*) B. Weber, C. Carbonera, C. Desplanches and J.-F. Létard, *Eur. J. Inorg. Chem.*, 2008, 1589; (*d*) B. Weber, E. S. Kaps, C. Desplanches, J.-F. Létard, K. Achterhold and F. G. Parak, *Eur. J. Inorg. Chem.*, 2008, 4891.

13 T. Pfaffeneder, W. Bauer and B. Weber, *Z. Anorg. Allg. Chem.*, 2010, **636**, 183.

14 B. Weber, *Coord. Chem. Rev.*, 2009, **253**, 2432.

15 Team of authors in *Organikum*, Wiley-VCH, Weinheim, 2004, vol. 22, p. 753.

16 L. Wolf and E.-G. Jäger, *Z. Anorg. Allg. Chem.*, 1966, **346**, 76.

17 E.-G. Jäger, E. Häussler, M. Rudolph and M. Rost, *Z. Anorg. Allg. Chem.*, 1985, **525**, 67.

18 (*a*) B. Weber, H. Görls, M. Rudolf and E.-G. Jäger, *Inorg. Chim. Acta*, 2002, **337**, 247; (*b*) B. Weber, *PhD Thesis*, University of Jena, 2002, Der Andere Verlag, Osnabrück, 2003.

19 (*a*) B. Heyn, B. Hipler, G. Kreisel, H. Schreer and D. Walter, *Anorganische Synthesechemie*, Springer Verlag, Heidelberg, 1986, 2 Auflage; (*b*) B. Weber, R. Betz, W. Bauer and S. Schlamp, *Z. Anorg. Allg. Chem.*, 2010, DOI: 10.1002/zaac.201000274/.

20 A. Altomare, M. C. Burla, G. M. Camalli, G. Cascarano, C. Giacovazzo, A. Guagliardi, A. G. G. Moliterni, G. Polidori, and R. Spagna, *SIR 97*, Campus Universitario Bari, 1997; A. Altomare, M. C. Burla, G. M. Camalli, G. Cascarano, C. Giacovazzo, A. Guagliardi, A. G. G. Moliterni, G. Polidori and R. Spagna, *J. Appl. Crystallogr.*, 1999, **32**, 115.

21 G. M. Sheldrick, *SHELXL 97*, University of Göttingen, Germany, 1993.

22 C. K. Johnson and M. N. Burnett, *ORTEP-III*, Oak-Ridge National Laboratory, Oak-Ridge, 1996; L. J. Farrugia, *J. Appl. Crystallogr.*, 1997, **30**, 565.

23 E. Keller, *SCHAKAL 99*, University of Freiburg, Germany, 1999.

24 W. Bauer and B. Weber, *Inorg. Chim. Acta*, 2009, **362**, 2341.

25 V. A. Money, J. Elhaik, I. R. Evans, M. A. Halcrow and J. A. K. Howard, *Dalton Trans.*, 2004, 65.

26 B. Weber, E. S. Kaps, K. Achterhold and F. G. Parak, *Inorg. Chem.*, 2008, **47**, 10779.

27 W. Bauer, W. Scherer, B. Weber, submitted.

28 (*a*) A. B. Koudriavtsev, A. F. Strassen, J. G. Haasnoot, M. Grunert, P. Weinberger and W. Linert, *Phys. Chem. Chem. Phys.*, 2003, **5**, 3676; (*b*) A. B. Koudriavtsev, A. F. Strassen, J. G. Haasnoot, M. Grunert, P. Weinberger and W. Linert, *Chem. Phys.*, 2003, **5**, 3666.

29 J. A. Real, A. B. Gaspar, V. Niel and M. C. Munoz, *Coord. Chem. Rev.*, 2003, **236**, 121.

30 C. F. Macrae, I. J. Bruno, J. A. Chisholm, P. R. Edgington, P. McCabe, E. Pidcock, L. Rodriguez-Monge, R. Taylor, J. van de Streek and P. A. Wood, *J. Appl. Crystallogr.*, 2008, **41**, 466.

31 H. Spiering, E. Meissner, H. Köppen, E. W. Müller and P. Gütlich, *Chem. Phys.*, 1982, **68**, 65.

32 G. Leibeling, *PhD Thesis*, University of Jena, Germany, 2003.

33 B. Weber, W. Bauer and J. Obel, *Angew. Chem., Int. Ed.*, 2009, **47**, 10098.

34 B. Weber, W. Bauer, T. Pfaffeneder, M. M. Dîrtu, Y. Garcia, manuscript in preparation.

35 B. R. Müller, G. Leibeling and E.-G. Jäger, *Chem. Phys. Lett.*, 2000, **319**, 368.

36 P. Guionneau, F. Le Gac, S. Lakhoufi, A. Kaiba, D. Chasseau, J.-F. Létard, P. Négrier, D. Mondieig, J. A. K. Howard and J.-M. Léger, *J. Phys.: Condens. Matter*, 2007, **19**, 326211.

37 J.-A. Real, B. Gallois, T. Granier, F. Suez-Panamá and J. Zarembowitch, *Inorg. Chem.*, 1992, **31**, 4972.

38 B. Gallois, J.-A. Real, C. Hauw and J. Zarembowitch, *Inorg. Chem.*, 1990, **29**, 1152.